Design and Control of a Photovoltaic Distribution System Based on Modular Buck-Boost Converters

Diseño y control de un sistema de distribución fotovoltaico basado en convertidores Buck-Boost modulares

Harrynson Ramírez-Murillo [ID][1], Carlos A. Torres-Pinzón [ID][2], Fabián Salazar-Cáceres [ID][3], Valentina Vera-Saldaña [ID][4], and Carlos J. Mojica-Casallas [ID][5]

ABSTRACT

The main contribution of this research is the design of a series hybrid topology for a photovoltaic distribution system using Buck-Boost converter modules. This design incorporates a maximum power point tracking (MPPT) algorithm based on the perturb and observe method, linear PI controllers, and an energy management algorithm. The controllers' design is validated through simulation using PSIM and SISOTOOL/MATLAB. This work aims to achieve active power sharing in the AC grid through a control loop implemented with a three-phase inverter. The validation of the topology and controller design demonstrates tracking and robustness in four test scenarios for the state variables in microgrids: constant and variable irradiance conditions, auxiliary storage device (ASD) protection and control loops, and power sharing with the AC grid, while considering the DC system dynamics.

Keywords: solar energy, DC-DC power converters, DC-AC power converters, microgrids, energy management systems

RESUMEN

La principal contribucion de este trabajo de investigacion es el diseño de una topologia hibrida en serie para un sistema de distribucion fotovoltaico, empleando modulos de convertidores Buck-Boost. Este diseño incorpora un algoritmo de seguimiento del punto de maxima potencia basado en el metodo perturbar y observar, controladores PI lineales y un algoritmo de gestion de energia. El diseño de los controladores se valida mediante simulacion en PSIM y SISOTOOL/MATLAB. El objetivo de este trabajo es el reparto de potencia activa en la red mediante un lazo de control implementado en un inversor trifasico. La validacion de la topologia y el diseño de controladores demuestra seguimiento y robustez en cuatro escenarios de prueba para las variables de estado en microrredes: condiciones de irradiancia constantes y variables, lazos de control y proteccion de dispositivos de almacenamiento auxiliar (ASD) y reparto de potencia en la red AC considerando la dinamica de los sistemas DC.

Palabras clave: energia solar, convertidores de potencia DC-DC, convertidores de potencia AC-DC, microrredes, sistemas de gestion de energia

Introduction

Non-conventional renewable energy sources (NCRES) are necessary for modern electricity systems, both in the National Interconnected System (NIS) and in non-interconnected zones (NIZ). This type of energy is indispensable for sustainable economic development, the reduction of greenhouse gases (GHG), and the energy security of the system. The latter has great relevance in countries of the Pacific and Caribbean Region, as the El Niño phenomenon and the effects of climate change tend to be increasingly relevant elements for the planning and operation of electrical power systems. Likewise, renewable energies contribute directly to Goal 7 of the Sustainable Development Goals (SDGs), which is related to *Affordable and Clean Energy* (Swain and Karimu, 2020).

Several reviews on AC and DC microgrid operation, applications, modeling, and control strategies have been presented in the literature Shahgholian (2021); Dragičević and Li (2018); Quintero-Molina *et al.* (2020); Gao *et al.* (2019). An advantage of using these networks is that they provide more reliability to the system, since they allow power generation to take place closer to the load centers. In addition, this increases the quality of the energy supplied. Likewise, microgrids can operate in two modes: island and normal (connected to the network). Considering the

vulnerability of electrical power systems, the island mode provides safety Luna *et al*. (2020).

DC microgrids have additional benefits, and they include reduced stages in the AC-DC interfaces required for residential loads. Both AC and DC microgrids operate autonomously, controlling parameters within the established limits. However, DC microgrids have a complex control architecture, mainly due to instantaneous power balance. The most important factors in their design are the generation-load power balance and the battery's state of charge (SOC) Hernández *et al*. (2021).

NCRES such as wind and solar photovoltaic (PV) generation could serve as a backup during El Niño events. There is a complementarity between hydroelectric resources and NCRES during drought periods. However, the massive implementation of NCRES constitutes drawbacks for operating electrical power systems according to their

[1] Universidad de La Salle, Bogotá D.C., Colombia. E-mail:haramirez@unisalle.edu.co
[2] Universidad Santo Tomás, Bogotá D.C., Colombia. E-mail:carlostorresp@usta.edu.co
[3] Universidad de La Salle, Bogotá D.C., Colombia. E-mail:jfsalazar@unisalle.edu.co
[4] Electrical engineer, ENEL, Colombia. E-mail: valentina.vera@utp.edu.co
[5] Universidad Santo Tomás, Bogot á D.C., Colombia. E-mail:carlosmojica@usta.edu.co

power and distribution levels, given the randomness of these primary resources. For a massive expansion of these distributed energy resources (DERs), it is essential to develop novel control functionalities that mitigate the large-scale impacts of these technologies Luna *et al.* (2020). In Hernández *et al.* (2021), an islanded microgrid for a rural area was designed and simulated in PSCAD/EMTDC. This design considered a battery to store energy when solar irradiance is low. In this research work, the SOC of the battery design uses the incremental conductance algorithm.

Rajanna (2022) designed a system consisting of a PV system with maximum power point tracking (MPPT), a battery storage system, and an improved three-level neutral point clamped (NPC) inverter. The NPC inverter accurately generates the required AC voltage via a modulation method for a three-level vector, particularly in the face of unbalanced DC voltages. This work evaluated the performance of the NPC inverter in different configurations, considering the SOC characteristics under varying solar irradiance levels.

Srikanth Goud and Sekhar (2023) presented a PV system connected to a DC-DC converter, which was then connected to a DC-link bus and converted to AC using an inverter before being fed into the grid. An optimization technique called *cuckoo search optimization* (CSO) *MPPT* maximized the generated power. The system was simulated in MATLAB/Simulink. The results indicate that the CSO approach outperforms the perturb and observe (P&O) and particle swarm optimization (PSO) approaches.

A Buck-Boost configuration with inductors coupled to the current control loop of a hybrid fuel cell system was shown in Ramírez-Murillo (2015). Despite the slow dynamics of proton-exchange membrane fuel cell (PEMFC) systems, this article is relevant because it considers the same scheme as DC-DC modular converters.

Restrepo *et al.* (2011) and Restrepo *et al.* (2012) presented the small-signal model and the experimental closed-loop transfer functions of the selected modular Buck-Boost converter. These works ease the simulation model by providing the gains and bandwidths for its inner current loops.

The main contribution of this research is a series hybrid (SH) topology design based on Buck-Boost converter modules, considering a PV source while implementing an MPPT algorithm based on the P&O method, synthesizing several linear PI controllers for the inner loops of a distributed generation system. These topology and control designs are validated through simulations on PSIM and SISOTOOL/MATLAB. The process is carried out on a 48 *V* and 768 *W* regulated DC distribution bus, designing a control loop for power-sharing to the AC grid while employing a three-phase inverter. The simulation model obtained for this microgrid is validated through the most relevant scenarios, testing the tracking and robustness properties of each loop.

This article is organized as follows. The Methodology section shows the DC-DC and DC-AC converters and the selected hybrid topology and the auxiliary storage device (ASD). Moreover, a design criterion is proposed for the energy management algorithm, and a linear state-space model for the converter is defined. In the Results section, a simulation is performed for a set scenarios, testing whether the state variables are suitable operation points. Then, a

discussion regarding the results is presented. In the final section, the conclusions and future works of this research are summarized.

Methodology

This section shows the design of the controllers that allow for energy management in the proposed microgrid (Figure 1). It consists of modular Buck-Boost converters and an ASD device, supervised via a master control. The control strategies for the solar array, the voltage regulation in the DC bus, and the control loops of the ASD system were tuned using SISOTOOL/MATLAB, whose design parameters are based on a minimum gain margin of 6 *dB* and a phase margin in the [30, 60]° range Ramírez-Murillo (2015).

To regulate the DC bus, this study considered the SH topology described in Ramírez-Murillo *et al.* (2014). Unlike that work, this research used an array of solar panels as a primary source, in which an MPPT algorithm was applied in order to ensure maximum power extraction. It is essential to highlight that the development of an on-grid-type microgrid requires the design of DC voltage control loops, in conjunction with controlling the active power injected into the grid via an inverter.

Modular converter

A Buck-Boost converter is a switched-mode converter whose output voltage can be higher, lower, or equal to the input voltage, as it can operate in three different modes: 1) *Buck mode*, where the input voltage is higher than the output voltage ($V_g > V_o$); 2) *Boost mode*, where the input voltage is lower than the output voltage ($V_g < V_o$); and 3) *Buck-Boost mode*, where the input voltage is approximately equal to the output voltage ($V_g \approx V_o$) Ramírez-Murillo (2015). Among the advantages of this type of converter are a high power conversion efficiency and the capability to control input/output currents.

The converter consists of a Boost stage in cascade, connected with a Buck stage with magnetically coupled inductors, with an included damping network. The scheme of a Buck-Boost converter with current sensors is shown in Figure 2. The damping branch consists of a series of resistances R_d and a capacitor C_d connected in parallel to the capacitor C_F Bendib *et al.* (2015).

The averaged model of the converter is represented by a set of differential equations that consider the damping network and the turns ratio $n = 1$, as described in Erickson and Maksimovic (2007), where d_1 and d_2 correspond to the cycles of the switches Q_1 and Q_2. Likewise, the overline in the variables corresponds to the average during a switching period. Likewise, linearizing the set of differential equations, in conjunction with the small-signal state vector given by Equation (1), the dynamic model is shown in Equation (2), where A is the state matrix, and B_1 and B_2 are the input vectors corresponding to $\tilde{d}_1$ and $\tilde{d}_2$. The state matrices are presented in Equation (3) Restrepo *et al.* (2011).

$$\tilde{x} = [\quad \tilde{i}_{Lm} \quad \tilde{i}_L \quad \tilde{v}_C \quad \tilde{v}_{Cd} \quad \tilde{v}_o \quad]^T \tag{1}$$

$$\frac{d\tilde{x}}{dt} = A\tilde{x} + B_1\tilde{d}_1 + B_2\tilde{d}_2 \tag{2}$$
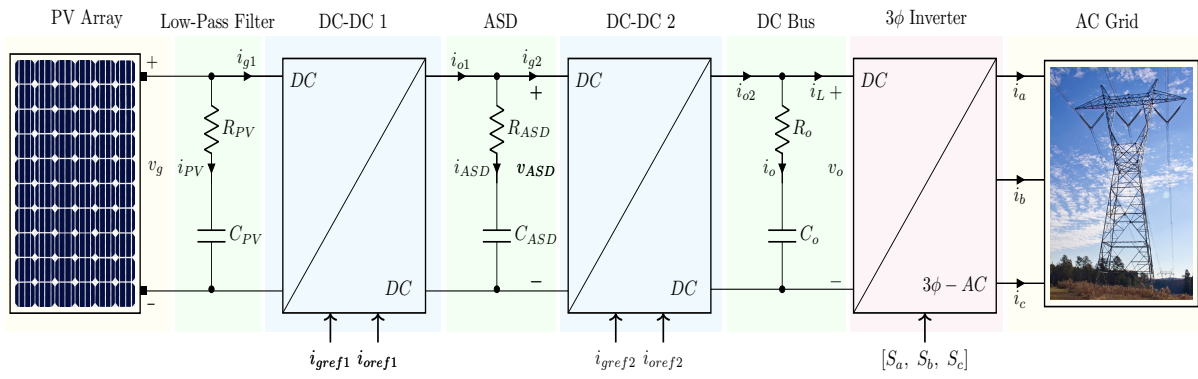
Figure 1: Proposed PV distribution system

Source: Authors
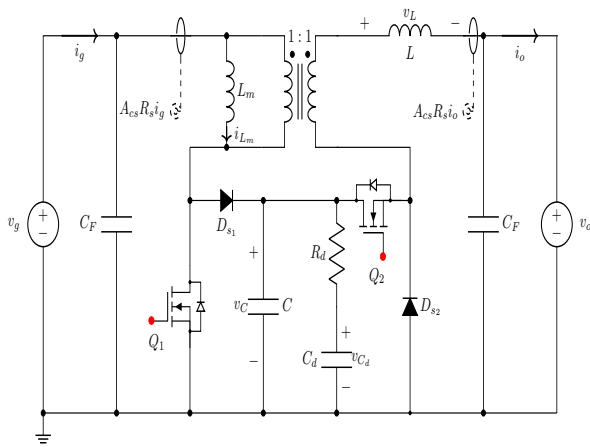
Figure 2: Buck-Boost converter schematic circuit

Source: Authors

$$A = \begin{bmatrix} 0 & 0 & \frac{D_1-1}{L_m} & 0 & 0 \\ 0 & 0 & \frac{D_2+D_1-1}{L} & 0 & \frac{-1}{L} \\ \frac{1-D_1}{C} & \frac{1-D_2-D_1}{C} & \frac{-1}{R_dC} & \frac{1}{R_dC} & 0 \\ 0 & 0 & \frac{1}{R_dC_d} & \frac{-1}{R_dC_d} & 0 \\ 0 & \frac{1}{C_o} & 0 & 0 & \frac{-1}{R_oC_o} \end{bmatrix} \tag{3}$$

$$B_1 = \begin{bmatrix} \frac{-V_g}{L_m(D_1-1)} & \frac{-V_g}{L(D_1-1)} & \frac{-V_gD_2^2}{CR_o(D_1-1)^2} & 0 & 0 \end{bmatrix}^T$$

$$B_2 = \begin{bmatrix} 0 & \frac{-V_g}{L(D_1-1)} & \frac{V_gD_2}{CR_o(D_1-1)} & 0 & 0 \end{bmatrix}^T$$

The transfer functions of the small-signal converter from the current control to the input/output current loops are presented in Figure 3. The corresponding parameters are $\tau_a = 3,3\ \mu s$, $\tau_b = 33\ \mu s$, $K_1 = 590\ (sA)^{-1}$, and $K_2 = 1298$ $(sA)^{-1}$ Restrepo *et al.* (2012).

The control variable $\tilde{u}$ shown in Figure 3 refers to the duty cycles of the MOSFETs of the modular converter, as seen in Equation (4).

$$\tilde{u} = \begin{cases} \tilde{d}_1(t) & \text{Boost Mode} \\ \tilde{d}_2(t) & \text{Buck Mode} \end{cases} \tag{4}$$
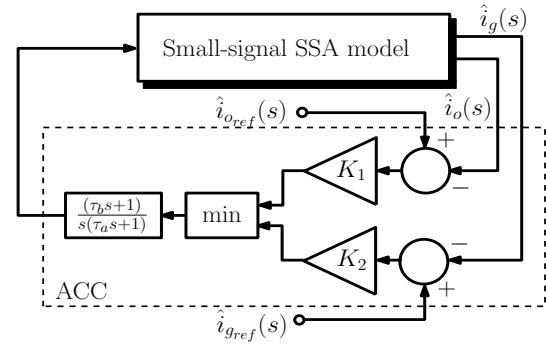
Figure 3: Block diagrams of the average current-mode control (ACC)

Source: Authors

DC bus voltage control loop design

In addition to the small-signal current control loop described in the previous subsection, it is necessary to add a voltage control loop to regulate the converter input/output voltages in each module. The closed-loop transfer function is presented in Equation (5), where ω_{ci} is the natural frequency, whose value is $2\pi8$ krad/s; and ζ is the damping factor, which corresponds to 0,44 Ramírez-Murillo (2015). These values were selected while aiming for the lowest damping factor and bandwidth values Restrepo *et al.* (2011).

$$H_i(s) = \frac{\tilde{i}_o(s)}{\tilde{i}_{oref}(s)} = \frac{\omega_{ci}^2}{s^2 + 2\zeta\omega_{ci}s + \omega_{ci}^2} \tag{5}$$

The European Cooperation for Space Standardization (ECSS) provides an output impedance mask for the DC bus criterion, which allows for a 1 % variation in the voltage v_o with a 50 % load disturbance i_o. This impedance is presented in Equation (6) Mourra *et al.* (2008).

$$Z_{DCBus} \leq \frac{0,01v_o}{0,5i_o} = \frac{0,02v_o}{i_o} = \frac{(0,02)(48)V}{16A} = 60\ m\Omega \tag{6}$$

The value of C_o is calculated using Equation (7).

$$\frac{1}{w_oC_o} \leq Z_{DCBus}. \tag{7}$$

Here, ω_o corresponds to the bus voltage loop cutoff frequency, where a small ESR value is obtained. A parallel

capacitor array was proposed in order to obtain a capacity of $2,35\ mF$, with a series resistance of $11,8\ m\Omega$. In addition, voltage regulation in the DC bus is performed by the voltage control loop shown in Figure (Figure 4).
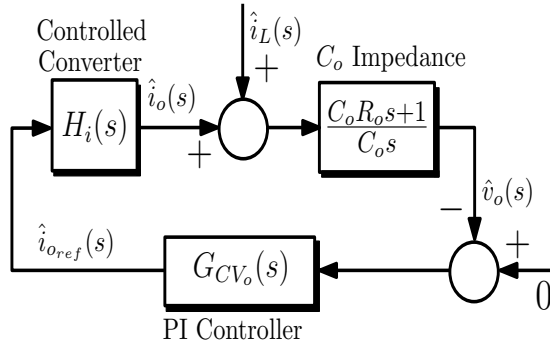
Figure 4: Small-signal model of the DC bus impedance

In the block diagram of Figure Figure 4, there is an algebraic simplification multiplying the numerator of the impedance C_o by the additional pole of the controller $G_{CV_o}(s)$. The DC bus impedance's closed-loop was adjusted on SISOTOOL with a bandwidth of $1,29\ kHz$, obtaining a proportional gain of $20,894\ kAs/V$ and a time constant τ equal to $890\ \mu s$.

Auxiliary storage device

A simplified lithium-ion battery (LIR18650, $2,6\ Ah$ model) was used in this work EEMB (2010). This model took into account only the nominal region of the discharge capacity, from Q_{top} to Q_{nom} values. Here, the energy management algorithm always works between the voltage ranges of E_{top} and E_{nom}. The main advantage of this model is that it is easy to obtain the parameters from the datasheet provided by the manufacturer. In the linear region, the battery model can be modeled as an RC series branch with a SOC in the $[20, 80]$ % range, where the C-value models the charging and discharging behaviors. The discharge behavior in the nominal region is required in order to size the energy storage. The area under the curve was obtained through Equation (8).

$$Energy = \frac{E_{top} - E_{nom}}{2}(Q_{nom} - Q_{top})Capacity(Ah)$$
$$Energy = \frac{3,8V + 3,5V}{2}(0,8 - 0,2)(2,6Ah) = 5,694\ J$$
(8)

The value of the capacitor for one cell was calculated via Equation (9).

$$E = \frac{C(E_{top}^2 - E_{nom}^2)}{2}$$
$$C = \frac{(5,694J)(2)}{(3,8^2 - 3,5^2)V} = 5,2\ F$$
(9)

However, to obtain the reference voltage of 48 V, an array of six branches connected in parallel was proposed. Each branch contains 14 cells connected in series. The capacitor value was obtained from Equation (9) while the series resistor value comes from the datasheet provided by the manufacturer EEMB (2010). The equivalent RC series

branch for the selected ASD is presented in Equation 10.

$$C_{ASD} = \frac{5,2}{14}(6) = 2,228\ F$$
$$R_{ASD} = \frac{(70m\Omega)(14)}{6} = 163\ m\Omega$$
(10)

ASD control loop design

The battery impedances were calculated for the following loops: 1) a nominal or reference SOC (20 %), 2) a minimum SOC (4 %), and 3) a maximum SOC (80 %). This is presented in Equation (11), considering the criteria established by the ECSS.

$$Z_{v_{ASDref}} \leq \frac{0,02v_{ASDref}}{i_{ASD}} = \frac{(0,02)(3,5V)(14)}{16} = 61,25\ m\Omega$$

$$Z_{v_{ASDmin}} \leq \frac{0,02v_{ASDmin}}{i_{ASD}} = \frac{(0,02)(3V)(14)}{16} = 52,5\ m\Omega \quad (11)$$

$$Z_{v_{ASDmax}} \leq \frac{0,02v_{ASDrmax}}{i_{ASD}} = \frac{(0,02)(3,8V)(14)}{16} = 66,5\ m\Omega$$

The controller parameters were obtained according to the previously mentioned DC bus impedance mask. The nominal and minimum SOC loops were adjusted while considering a bandwidth of $0,00307\ kHz$, a proportional gain of $11,488\ As/V$, and a time constant τ of $2,9\ s$. The maximum SOC loop was set with a bandwidth of $0,00318\ kHz$, a proportional gain of $6,9632\ As/V$, and a time constant τ of $5\ s$.

Maximum power point tracking loop

The panel filter has the same RC parameters $C_o = C_{PV}$ and $R_o = R_{PV}$ as the DC bus. However, the value of the impedance mask changes, as seen in Equation (12).

$$Z_{v_g} \leq \frac{0,02v_{gmin}}{i_{PV}} = \frac{(0,02)(60V)}{16A} = 37,5\ m\Omega \quad (12)$$

The PI controller parameters were adjusted via SISOTOOL with a $0,903\ kHz$ bandwidth, given a proportional gain of $11,802\ kAs/V$ and a time constant τ of $1,1\ ms$. On the other hand, the MPPT control loop was tuned considering the P&O algoritm, where, if $\Delta V > 0$, then the voltage is increased by $0,1\ V$. On the other hand, if $\Delta V < 0$, then the voltage is decreased by $0,1\ V$ Mohan *et al.* (2003).

Power sharing algorithm

A three-phase inverter is a key device for interfacing a DC system with an AC grid. The switching of the insulated-gate bipolar transistors (IGBTs) is performed by comparing each of the three current and voltage sine waves, which are obtained after the pulse-width modulation (PWM). These waves have a $120°$ phase shift, with the same triangular carrier signal and switching frequency of $15\ kHz$. Likewise, the output amplitude is determined by the ratio of the signal carrier to the modulator. The inverter output voltage requires a step-up transformer with a Delta-Star connection and a grounded neutral wire. Thus, the inverter will be able to inject any current level into the grid. On the other hand, the $230\ V$ line's voltage regulation is achieved by modulating the pulse width to obtain the switching signals $[S_a, S_b, S_c]$. The design criteria are described below.

A series RL first-order low-pass filter is required to eliminate the transmission line current ripple. Its transfer function is

presented in Equation (13). These parameters correspond to R_{abc} and L_{abc}.

$$G_{abc}(s) = \frac{1}{R_{abc}L_{abc}s + 1} = \frac{1}{0,0003183s + 1} \quad (13)$$

The Park transform allows converting the sinusoidal values in time into steady-state values, and it is applied to both the filtered currents and the grid voltages. It is important to consider that the phase of the grid starts at $t = 0\ s$. Likewise, this transform reduces the harmonic content of the output voltage in the inverter.

Active power control is carried out by calculating the reference currents through the network voltages in a steady state. The current references for the PI regulator are obtained via Equation (14) from the active and reactive power reference values, which corresponds to $P_{ref} = (16)(48)\ W = 768\ W$ and $Q_{ref} = 0\ VAR$, respectively, and the voltage references v_d and v_q.

$$i_{dref} = \frac{2}{3} \frac{P_{ref}V_d + Q_{ref}V_q}{V_d^2 + V_q^2}$$

$$(14)$$

$$i_{qref} = \frac{2}{3} \frac{P_{ref}V_q + Q_{ref}V_d}{V_d^2 + V_q^2}$$

The PI controller was adjusted using the SmartCtrl tool of PSIM. The GM of the PI controller and the BW were set to $45,33°$ and $478,63\ Hz$, respectively.

Results

Constant load under variations in the irradiance profile

In this subsection, three control loops are designed and validated: first, the DC bus voltage is regulated at $V_{oref} = 48\ V$ using a reference current i_{oref2}; second, the panel minimum voltage is regulated at $V_{gmin} = 30\ V$ through i_{gref1} and the MPPT algorithm; finally, the ASD $V_{ASDref} = 48\ V$ nominal voltage is also controlled by applying the i_{gref1} signal. These control input currents regulate the voltages v_g and v_o in the distribution system shown in Figure 5. In this simulation, a constant commercial load value of $3,3\ \Omega$, $698\ W$ was obtained.

In Figure 5a, an amplitude-varying irradiance profile is depicted, considering values of $[600, 1000]\ W/m^2$. During the interval from 0 to t_1, the PV array fully supplies the power demand, as shown in Figure 5b. However, when the irradiance decreases at $t_1 = 100\ ms$, the array cannot supply all the power required. Therefore, the ASD supplies the power shortage demand. This system continues supplying power from t_1 to t_2, while the power demand increases. Subsequently, in the intervals from t_2 to t_3 and from t_3 to t_4, the PV array power is set to a reference, at 310 and 414 W, which corresponds to irradiance levels of 600 and 800 W/m^2, respectively. Finally, from t_4 to t_5, once the system reaches the maximum irradiance value of $1000\ W/m^2$, the PV array power stabilizes at a constant power demand. It is observed that, from 0 to t_4, the maximum PV power is supplied. Moreover, from t_4 to t_5, the total power required by the load is delivered by the ASD, and the energy management algorithm prioritizes the ASD nominal voltage control loop at $V_{ASDref} = 48\ V$.
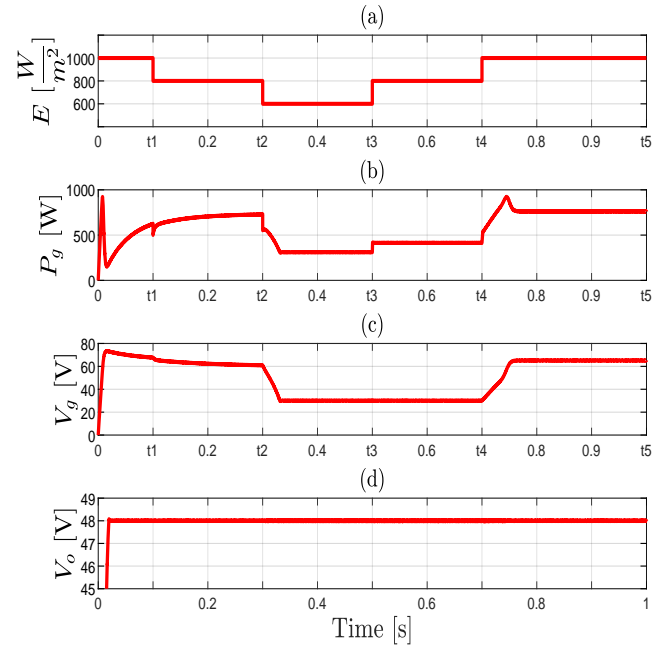
**Figure 5:** (a) Test irradiance profile, (b) input power, (c) PV array voltage, and (d) DC bus voltage

Source: Authors

In Figure 5c, once the irradiance decreases, the voltage also decreases, until it stabilizes at $V_{gmin} = 30\ V$, as shown for the time interval from t_2 to t_4, which regulates the PV array voltage at the minimum operating value. On the other hand, from t_4 to t_5, when the irradiance increases to $1000\ W/m^2$, the panel voltage reaches $65\ V$ in order to provide the total demanded power. In Figure 5d, the DC bus voltage behavior is shown at the reference value of $V_{oref} = 48\ V$ and under a $3,3\ \Omega$ constant load, maintaining this state regardless of variations in demanded power and irradiance.

Impedance-varying load profile under a constant irradiance condition

In this scenario, two control loops are validated: first, the DC bus voltage regulation loop at $V_{oref} = 48\ V$ through I_{oref2}; and second, the ASD nominal voltage regulation at $V_{ASDref} = 48\ V$ using I_{gref1} and the MPPT algorithm. These control loops are tested while considering a constant impedance load of $20\ \Omega$, adding a variable impedance load of $3,9\ \Omega$.

Figure 6a shows that, under a constant irradiance of $1000\ [W/m^2]$, the input power is stabilized at $410\ W$. Moreover, in Figure 6b, the output voltage V_g is stabilized through the MPPT algorithm, reaching the maximum power point and with no significant increases or decreases in the input voltage. Figure 6c validates the DC bus voltage regulation loop. Finally, in Figure 6d, there are DC bus voltage ripples of $1\ V$ throughout $0,1\ s$. This disturbance in the load represents a demanding scenario, with $76,92\ \%$ of the maximum power, which corresponds to $768\ W$.
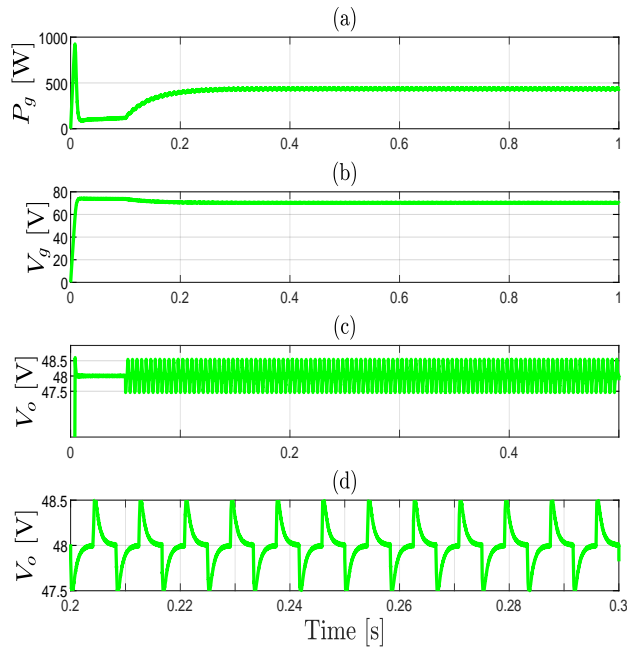
Figure 6: (a) Input power; (b) PV array voltage; (c) DC bus voltage, large signal model; and (d) small-signal variations of the DC bus voltage
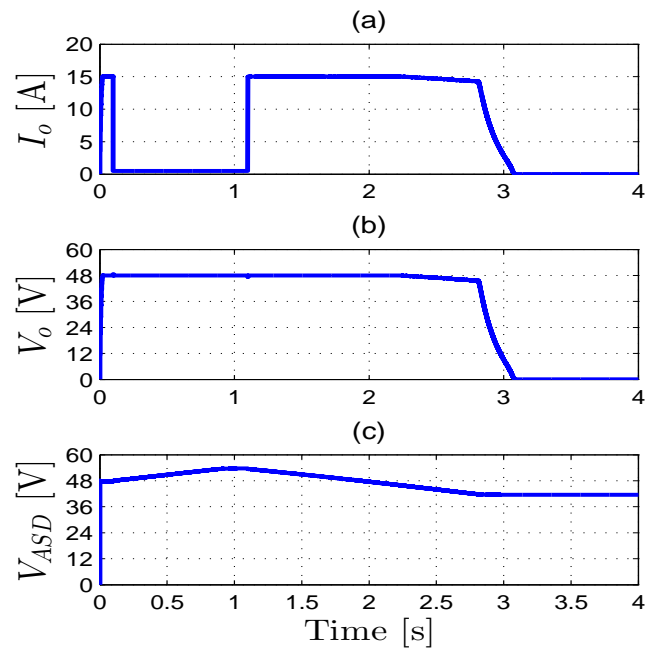
Source: Authors

ASD loops scenario test

In this scenario, three control loops are validated: the DC bus voltage, which has been widely considered in the previous subsections; the ASD minimum voltage at $V_{ASDmin} = 42\ V$ using I_{gref2}; and the ASD maximum voltage at $V_{ASDmax} = 53,2\ V$ using I_{oref1}, which implies an MPPT algorithm failure.

Figure 7a shows a saturation of the current reference $I_{gref1} = 16\ A$, with an initial constant load of $3,2\ \Omega$ until $t = 0,1\ s$. Then, from $t = 0,1$ to $t = 1,1\ s$, the maximum ASD voltage V_{ASDmax} exhibits the required performance, while a load shedding is deployed, considering a constant load of $100\ \Omega$. On the other hand, from $t = 1,1\ s$ onward, the load is fully reconnected and shows an adequate behavior in the current output. Finally, Figure 7b shows the DC bus voltage drop V_{oref}, while the ASD minimum reference voltage V_{ASDmin} achieves the reference value in Figure 7c.

Inverter considering the DC system dynamics

In this scenario, the dynamics of the DC system are included using a square signal, whose maximum and minimum values correspond to 768 and $115,2\ W$, respectively. This profile is shown in Figure 8a, whuch includes the active power control loop mentioned in the previous section. Figures 8b and 8c illustrate the three-phase voltages ($V_g = [v_a,\ v_b,\ v_c]^T$) and currents ($I_g = [i_a,\ i_b,\ i_c]^T$) after considering the DC dynamics.

Figure 7: (a) DC bus current, (b) DC bus voltage, and (c) battery voltage
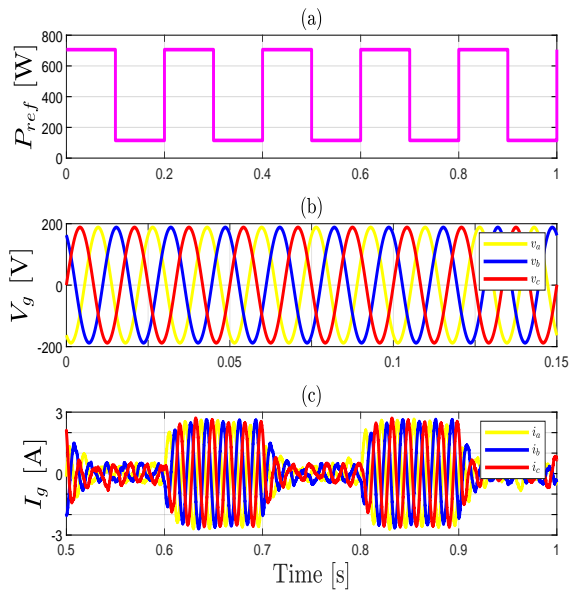
Source: Authors

Discussion

In the previous section, the results obtained for the microgrid were compared with the findings of another study Rajanna (2022), where it was observed that the maximum and minimum SOC of the ASD were not regulated, thus requiring the incorporation of additional protection loops. Furthermore, another recent work Srikanth Goud and Sekhar (2023) highlighted the absence of an ASD. To address these limitations, this study focused on establishing parameters for the protection and operation loops of the ASD. Additionally, an energy management algorithm with an increased number of control loops was designed, using a versatile modular Buck-Boost converter. To regulate the voltages of the buses while considering the power variations, the design of the control loops in the DC stage employed the impedance mask criterion. Moreover, the injection of active power into the AC grid was regulated through the dq model of the inverter. As a remark, the P&O algorithm was integrated into the control loop that regulates the voltage V_g.

Other recent works Zhou *et al.* (2022); Shang *et al.* (2020) explored the optimization of ASDs in microgrids. These studies proposed a novel approach that integrates machine learning techniques with power management algorithms to enhance the efficiency and performance of ASD. Reinforcement learning techniques proved to be effective through simulations and experimental validations, exhibiting significant improvements in energy management and system performance Ali *et al.* (2021).

Conclusions

The main contribution of this research is the design of a series hybrid (SH) topology for a PV distribution system, using two modular Buck-Boost converters.

Figure 8: (a) Reference power from DC dynamics, (b) three-phase voltages, and (c) three-phase currents

Source: Authors

These converters allow designing an energy management algorithm, where MPPT, nominal SOC, and maximum ASD SOC control loops are considered for the first module. Likewise, the second stage ensures the minimum SOC and the DC bus voltage reference, as shown in the simulation results. Four test scenarios were proposed to validate the correct operation of the system control loops.

The ASD simplified model drives a suitable transient and shows a steady-state behavior. As a result, when the microgrid is connected to the AC grid (on-grid), the designed energy management scheme allows supplying the demand under irradiance variations. The power injected into the AC grid is controlled using a three-phase inverter, but its waveform is distorted. Therefore, it is recommended that a harmonic compensation device be introduced, such as passive or active filters, line reactors, and hybrid filters, among others.

The impedance mask criterion allows appropriately designing classical controllers for voltage regulation in DC buses, wherein the impedance is modeled. Likewise, the modular converter used in this research facilitates voltage regulation, as it allows for input/output current control with a higher bandwidth. The interaction between these loops does not entail any conflict, given that their control hierarchy goes hand in hand with the lowest energy consumption in the system.

CRediT author statement

All authors: conceptualization, methodology, software, validation, formal analysis, investigation, writing (original draft, writing, re-view, and editing), data curation.

Acknowledgements

References

Ali, K. H., Sigalo, M., Das, S., Anderlini, E., Tahir, A. A., and Abusara, M. (2021). Reinforcement learning for energy-storage systems in grid-connected microgrids: An investigation of online vs. offline implementation. *Energies*, *14*(18), 5688. https://doi.org/10.3390/en14185688.

Bendib, B., Belmili, H., and Krim, F. (2015). A survey of the most used mppt methods: Conventional and advanced algorithms applied for photovoltaic systems. *Renewable and Sustainable Energy Reviews*, 45:637–648. https://doi.org/10.1016/j.rser.2015.02.009.

Dragičević, T. and Li, Y. (2018). Ac and dc microgrid control. In *Control of Power Electronic Converters and Systems*, pages 167–200. https://doi.org/10.1016/B978--0--12--816136--4.00018--X. Elsevier.

EEMB (2010). *Lithium-ion battery data sheet*. EEMB Co.

Erickson, R. W. and Maksimovic, D. (2007). *Fundamentals of power electronics*. Springer Science & Business Media.

Gao, F., Kang, R., Cao, J., and Yang, T. (2019). Primary and secondary control in dc microgrids: a review. *Journal of Modern Power Systems and Clean Energy*, 7(2):227–242. https://doi.org/10.1007/s40565--018--0466--5.

Hernández, E. D. G., Aldana, N. L. D., and Hernández, A. C. L. (2021). Energy management electronic device for islanded microgrids based on renewable energy sources and battery-based energy storage. *Ingeniería e Investigación*, 41(1):1–5. https://doi.org/10.15446/ing.investig.v41n1.86047.

Luna, A. C., Díaz, N. L., and Narvaez, E. A. (2020). Optimal coordination of active generators in a grid-connected microgrid. *Ingeniería e Investigación*, 40(3):47–54. https://doi.org/10.15446/ing.investig.v40n3.82665.

Mohan, N., Undeland, T. M., and Robbins, W. P. (2003). *Power electronics: converters, applications, and design*. John Wiley & Sons.

Mourra, O., Blancquaert, T., Signorini, C., and Tonicello, F. (2008). European cooperation for space standardization – The new standard for electric and electronic ECSS-E-ST-20-C [Conference presentation]. 8th European Space Power Conference.

Quintero-Molina, V., Blanco, A. M., Romero-L, M., Meyer, J., and Pavas, A. (2020). Power quality in ac islanded microgrids: Technical framework and state of the art review. *Ingeniería e Investigación*, 40(3):29–37. https://doi.org/10.15446/ing.investig.v40n3.89091.

Rajanna, B. V. (2022). Grid connected solar pv system with mppt and battery energy storage system. *International Transactions on Electrical Engineering and Computer Science*, 1(1):8–25. https://iteecs.com/index.php/iteecs/article/view/5.

Ramírez-Murillo, H. (2015). *Diseño, supervisión y control de sistemas híbridos pemfc*. [PhD thesis, Universitat Rovira i Virgili].

Ramírez-Murillo, H., Restrepo, C., Calvente, J., Romero, A., and Giral, R. (2014). Energy management dc system based on current-controlled buck-boost modules. *IEEE Transactions on Smart Grid*, 5(5):2644–2653. https://doi.org/10.1109/TSG.2014.2330198.

Restrepo, C., Calvente, J., Romero, A., Vidal-Idiarte, E., and Giral, R. (2011). Current-mode control of a coupled-inductor buck–boost dc–dc switching converter. *IEEE Transactions on Power Electronics*, 27(5):2536–2549. https://doi.org/10.1109/TPEL.2011.2172226.

Restrepo, C., Konjedic, T., Calvente, J., Milanovic, M., and Giral, R. (2012). Fast transitions between current control loops of the coupled-inductor buck–boost dc–dc switching converter. *IEEE transactions on power electronics*, 28(8):3648–3652. https://doi.org/10.1109/TPEL.2012.2231882.

Shahgholian, G. (2021). A brief review on microgrids: Operation, applications, modeling, and control. *International Transactions on Electrical Energy Systems*, 31:e12885]https://doi.org/10.1002/2050--7038.12885.

Shang, Y., Wu, W., Guo, J., Ma, Z., Sheng, W., Lv, Z., and Fu, C. (2020). Stochastic dispatch of energy storage in microgrids: An augmented reinforcement learning approach. *Applied Energy*, 261:114423. https://doi.org/10.1016/j.apenergy.2019.114423.

Srikanth Goud, B. and Sekhar, G. C. (2023). Cuckoo search optimization mppt technique for grid connected photovoltaic system. *International Transactions on Electrical Engineering and Computer Science*, 2(1):14–19, https://iteecs.com/index.php/iteecs/article/view/3.

Swain, R. B. and Karimu, A. (2020). Renewable electricity and sustainable development goals in the eu. *World Development*, 125:104693. https://doi.org/10.1016/j.worlddev.2019.104693.

Zhou, K., Zhou, K., and Yang, S. (2022). Reinforcement learning-based scheduling strategy for energy storage in microgrid. *Journal of Energy Storage*, 51:104379, https://doi.org/10.1016/j.est.2022.104379.